Journal of Alloys and Compounds 505 (2010) 235–238

Contents lists available at ScienceDirect

Journal of Alloys and Compounds

journal homepage: www.elsevier.com/locate/jallcom

Synthesis and characterization of the nanometric Pr-doped ceria

B. Matovic[a,*], S. Boskovic[a], M. Logar[b], M. Radovic[c], Z. Dohcevic-Mitrovic[c], Z.V. Popovic[c], F. Aldinger[d]

[a] Institute of Nuclear Sciences "Vinca," 11001 Belgrade, Serbia
[b] Faculty of Mining and Geology, Belgrade, Serbia
[c] Institute of Physics, Pregrevica, 11080 Belgrade, Serbia
[d] Max-Planck Institute, PML, Stuttgart, Germany

ARTICLE INFO

Article history:
Received 19 April 2010
Received in revised form 7 June 2010
Accepted 10 June 2010
Available online 18 June 2010

Keywords:
Ceria solid solution
XRD measurements
Raman spectroscopy
Red pigments

ABSTRACT

In this paper nanometric powders of solid solution of the host compound ceria (CeO_2) with Pr dopant in the lattice were synthesized by self-propagating room temperature (SPRT) synthesis with composition ($Ce_{0.9}Pr_{0.1}O_{2-\delta}$). Powder properties such as specific surface area crystallite and particle size and lattice parameters have been studied. BET, TEM, X-ray diffraction (XRD) analysis and Raman scattering measurements were used to characterize the samples at room temperature. Obtained solid solution exhibits a fluorite-type crystal structure. The average crystallite size is about 3–4 nm. Williamson–Hall plots were used to separate the effect of the size and strain in the nanocrystals. It is noticed the redshift and asymmetric broadening of the Raman F_{2g} mode which is explained with nanocrystalline nature of powders.

Color characters of solid solution depending on calcinations temperature and their position in the chromaticity diagram were studied by UV–vis spectrophotometry (diffuse reflectance).

1. Introduction

The study on production of red ceramic pigments with high temperature stability is of great importance to the ceramic industry [1]. At present, the following classical red pigments used on a large scale are: iron oxide (Fe_2O_3) encapsulated in zircon ($ZrSiO_4$) matrix and lead oxide (Pb_3O_4) in tin oxide (SnO_2) matrix give pale red or pink colors [2]. The red–orange pigments in the $Cd(S_xSe_{1-x})$–$ZrSiO_4$ system, and sodium urinate are toxic and unstable above 900 °C [3]. Another possibility for obtaining red pigments is to use ceria (CeO_2) doped with praseodymium (Pr^{4+}) ions that leads to a stable dye [4–6].

Today, production in the ceramic pigments is focused on high surface area powders, since this feature influences the color intensities. Thus, there is a great interest on development of nanosized pigments. Among the processes available for synthesizing nanometric ceramic powders [7–11], one of the methods that are cost and time effective is the self-propagating room temperature (SPRT) synthesis. SPRT procedure is based on the self-propagating room temperature reaction between metal nitrates and sodium hydroxide. This reaction is spontaneous and after being initiated it terminates extremely fast [12,13].

In this paper we present a study on the synthesis of nanometric Pr-doped ceria by SPRT method as well as its structural and optical properties from room temperature to 600 °C.

Apart from the interest to get more fundamental knowledge on the characteristics of solid solutions under study, it is also of interest to find out if the applicability of the Pr-doped ceria in pigments will be of practical interest. It is interesting to note that the influence of particle size on color hue was not studied in detail till now.

2. Experimental

Starting reactants used in the experiments were cerium nitrate hexahydrate ($Ce(NO_3)_3{\cdot}6H_2O$, Merck), praseodymium nitrate hexahydrate ($Pr(NO_3)_3{\cdot}6H_2O$, John Mathey) and sodium hydroxide (NaOH, Zorka Sabac). Amounts of nitrates and NaOH were calculated according to the nominal composition of the $Ce_{0.9}Pr_{0.1}O_2$ solid solution and reaction:

$$2|(1–0.9)Ce(NO_3)_3{\cdot}6H_2O + 0.9Pr(NO_3)_3{\cdot}6H_2O| + 6NaOH + (½–y)O_2 \rightarrow 2Ce_{0.9}Pr_{0.1}O_{2-y} + 6NaNO_3 + 15H_2O + 3/2O_2\uparrow \quad (1)$$

The chemicals were hand-mixed in alumina mortar for 5 min. After being exposed to air for 3 h, the mixture was suspended in water. Rinsing of $NaNO_3$ was performed in centrifuge Megafuge 1.0, Heraeus, at 3500 rpm for 10 min. This procedure was performed three times with distilled water and twice with ethanol. After analyzing the sodium content it was found to be in the ppm region. After drying at 70 °C for 24 h, powder was heat treated at 200, 400 and 600 °C for 15 min in ambient atmosphere.

Crystal structure was identified by X-ray diffraction (XRD) using filtered Cu Kα radiation (Siemens D5000). XRD was also used to evaluate the crystallite size and lattice parameters as a function of temperature. Assuming that the line broadening ($\beta = \beta' + \beta''$) is the sum of the contributions attributed to the crystalline size (c_s) and the strain (ε), which can be written as $\beta' = 1/(c_s \cos\theta)$ and $\beta'' = 4\varepsilon \tan\theta$, than

* Corresponding author.
E-mail address: mato@vinca.rs (B. Matovic).

0925-8388/$ – see front matter © 2010 Elsevier B.V. All rights reserved.
doi:10.1016/j.jallcom.2010.06.036

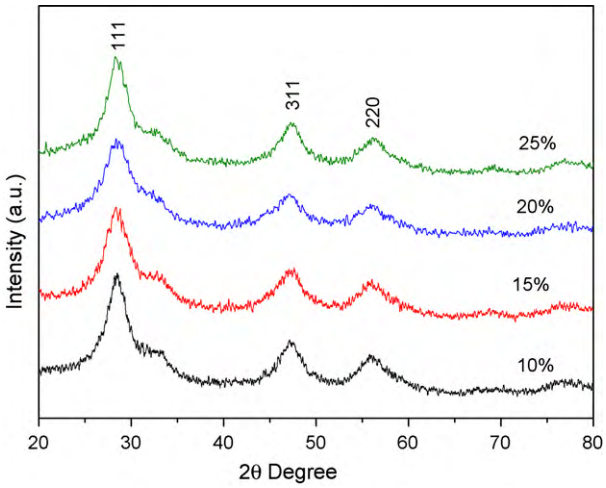

Fig. 1. X-ray diffraction patterns of $Ce_{1-x}Pr_xO_{2-\gamma}$ powders ($x = 0.1$, 0.15, 0.20 and 0.25).

the crystallite size and the strain can be determined from the linear relationship between $\beta\cos\theta$ and $4\sin\theta$, where θ is the Bragg diffraction angle, and strain (ε) is $\varepsilon = \Delta d/d$ (Δd is displacement of the lattice) [14]. Before measurement the angular correction was done by high quality Si standard. Lattice parameters were refined from the data using the least square procedure. Standard deviation was about 1%.

The Raman spectra were obtained using a U-1000 (Jobin-Ivon) double monochromator in back scattering geometry. The Raman spectra were excited by the 514 nm line of an Ar^+ ion laser and taken at room temperature. In order to avoid sample heating we used a cylindrical focus and the laser power was kept lower than 10 mW.

The adsorption characteristics of synthesized and annealed samples were determined. Adsorption and desorption isotherms of N_2 were measured at −196 °C using the gravimetric McBain method. The specific surface area, S_{BET}, for the samples, was calculated from the isotherms.

TEM analysis was performed on JEOL 400 FX instrument. Particle sizes were measured on micrographs directly after they were taken by using the existing computer programme Program Digital Micrograph.

Diffuse reflectance spectra were recorded on the computer controlled monochromator (Beckman DU) using p.a. $BaSO_4$ as a reference. The chopped signal (MC 1000A Thoealbs), synchronized and amplified by lock-in amplifier (LiA100 Thoralbs), was recorded. The color characteristics of specimens were calculated according to the CIE $L^*a^*b^*$ (1976) standard, using illuminant C spectral energy distribution.

3. Results and discussion

Typical X-ray diffraction patterns for the Pr-doped ceria are shown in Fig. 1. All of them are single phase, which are independent of dopant concentration in the range investigated. Peaks related to isolated Pr-phases are not observed and all of solid solution powders exhibit the fluorite crystal structure. This high solubility may be attributed to nanometric nature of powders. XRD analysis reveals that all peaks for each sample were significantly broadened indicating small crystallite size and/or strain.

Representative transmission electron microscope (TEM) image of the as-synthesized Pr-doped ceria reveals that particles are uniform with size between 3 and 4 nm (Fig. 2).

Since the all powders are nanometric, we chose only ceria solid solution with 10 at.% of Pr ($Ce_{0.9}Pr_{0.1}O_2$) for investigation. Behavior of this solid solution at different annealing temperatures is shown in Fig. 3. XRD analysis reveals that all peaks for each sample were significantly broadened indicating small crystallite size and/or strain. It is especially true for powder that is not annealed. It exhibits very diffuse diffraction lines, in such way that some atomic planes are impossible to indicate (*hkl*: 200, 400, 311, 420). However, annealed powders depict sharpened diffraction lines resulting from increasing the crystallite size.

The unit cell parameter a_o (Å) and crystallite size for $Ce_{0.9}Pr_{0.1}O_2$ at different temperatures are shown in Table 1. It was found that lattice parameter of nanomaterials obtained at 25 °C and annealed at 400 °C are higher with respect to bulk material [15,16]. This behavior can be ascribed to existence of the microstrain field originated from a vacancy clusters due to the presence of Ce^{3+} in undoped ceria [17]. Also, it is consistent with the substitution of Ce^{4+} ions in the lattice with Pr^{3+} ions (the ionic radii of Pr^{3+}, Pr^{4+} and Ce^{4+} are 1.126, 0.90 and 0.97 Å, respectively for eight-fold coordination) [18]. Thus, the expansion of the lattice with decreasing particle size

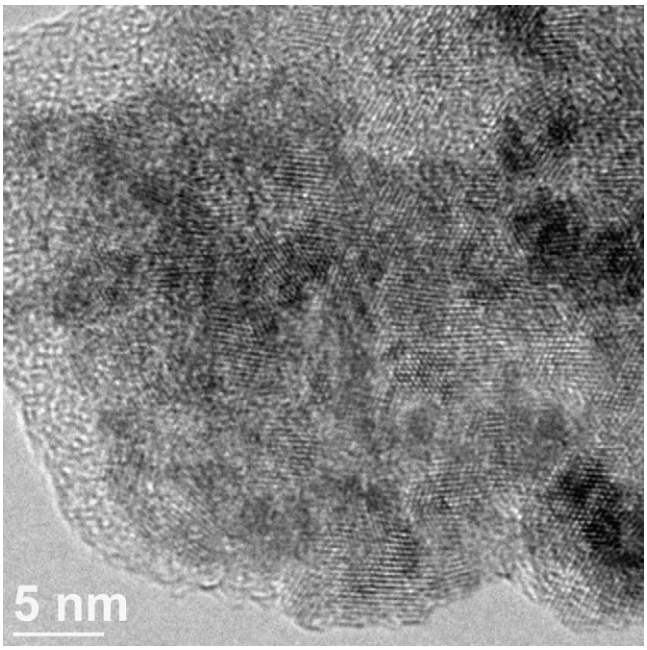

Fig. 2. TEM image of the as-synthesized Pr-doped ceria.

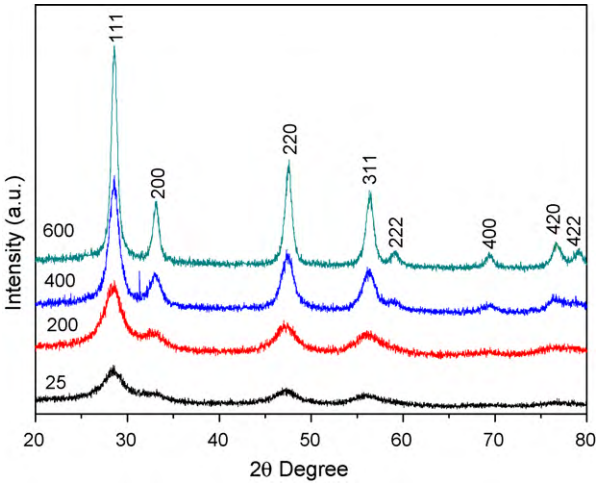

Fig. 3. Room temperature XRD of $Ce_{0.9}Pr_{0.1}O_2$ samples heat treated at different temperature for 15 min.

Table 1
Lattice parameter, crystallite size, strain and specific surface area of $Ce_{0.9}Pr_{0.1}O_2$ samples in function of temperature.

Temperature (°C)	Crystalline size (nm)	Lattice parameter (nm)	Strain ε	Specific surface area (m^2/g)
25	3.1	0.54482	0.0044	105
200	4.4	0.54387	0.0037	77
400	4.5	0.54202	0.0028	70
600	10.7	0.54087	0.0019	49

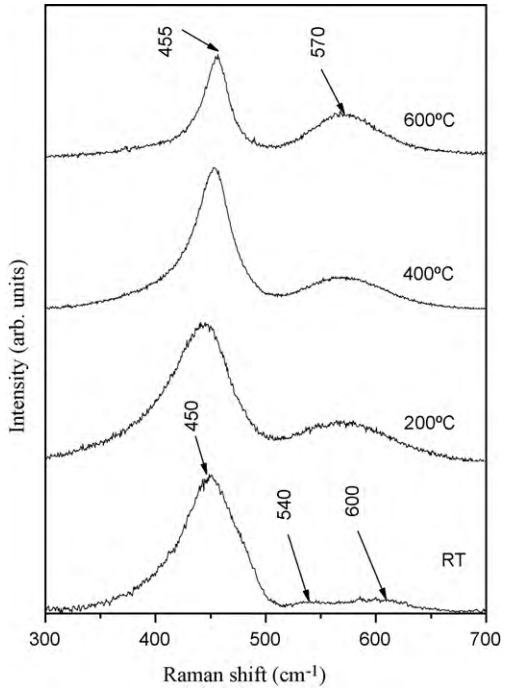

Fig. 4. Raman spectra of $Ce_{0.9}Pr_{0.1}O_2$ samples before and after heat-treated to 600 °C.

of doped ceria is due to presence of the larger concentration of oxygen vacancies due to presence of both Ce^{3+} and Pr^{3+} ions. However, heating at elevated temperature resulted in normal value of lattice parameters indicating the valance change from Ce^{3+} to Ce^{4+} and possibly Pr^{3+} to Pr^{4+} due to higher thermodynamic stability of Ce^{4+} and Pr^{4+} at higher temperature in ambient atmosphere. On the other hand, in annealed samples strong influence of temperature on strain and specific surface area is obvious. It is shown that smaller crystallite size displays higher strain. During annealing, crystallite size increases with lowering the strain.

Raman spectra are in agreement with the XRD analysis. Fig. 4 shows Raman spectra of $Ce_{0.9}Pr_{0.1}O_2$ samples before and after heat treatment up to 600 °C. Main feature of the first order Raman spectrum of CeO_2 is an F_{2g} mode located at 465 cm^{-1} in the bulk sample. In as-prepared samples this mode is shifted to lower energies (450 cm^{-1}), with increased line width and pronounced asymmetry at low energy side. Nanosized effects like phonon confinement, strain and nonstoichiometry can contribute to the observed changes in Raman peak profile [19]. After annealing Raman mode is shifted to higher frequencies 455 cm^{-1}, its line width is reduced down to 5 cm^{-1} and became more symmetric, which confirmed that thermally treated sample has lead to grain growth and better order structures. Additional modes can be observed at 540 and 600 cm^{-1} in spectrum taken before temperature treatment. These modes are assigned to extrinsic and intrinsic oxygen vacancies generated in CeO_2 lattice with doping and reduction in particle size, respectively. With increasing temperature of treatment these modes merge becoming one mode at 570 cm^{-1} that the intensity increases as temperature increases. The reason for the formation of the Raman mode at 570 cm^{-1} is due to substitution of two Ce^{4+} ions by two Pr^{3+} ions when one oxygen vacancy is introduced into the ceria lattice in order to maintain the electrical neutrality. Thus the band at 570 cm^{-1} might be linked to lattice defect that results in the creation of oxygen vacancies.

The reflectance curves show the absorption difference between as-prepared and annealed samples. For sample that was not thermally treated, an intense reflectance occurred along the full range

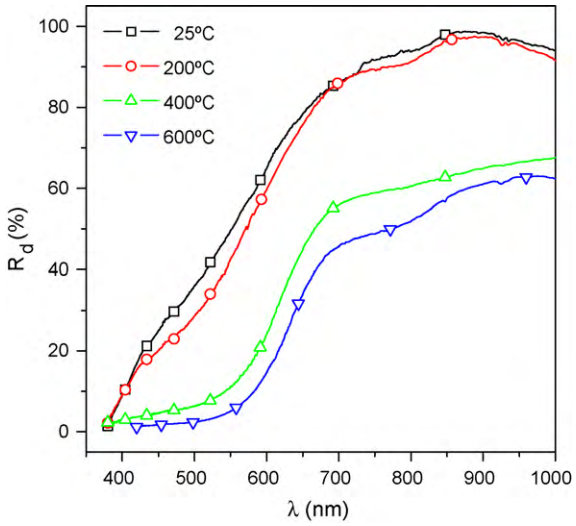

Fig. 5. The effect of annealing temperature on the color of the $Ce_{0.9}Pr_{0.1}O_2$ pigment powders.

of electromagnetic spectrum, which is opposite to the narrow reflectance range for the samples annealed at 400 and 600 °C (Fig. 5). It is obvious that increasing temperature results in increasing absorption and shifting the absorption edge towards lower energy. According to this observation there is a change of band gap and color characteristic of samples (Table 2). Band gap width decreases with temperature increasing. The biggest value of band gap possesses sample, which is not thermally treated. This is in good agreement with literature data [20]. Sample annealed at 200 °C exhibits a small reduction of band gap. The greatest band gap energy drop is observed between 200 and 400 °C. It is interesting that sample annealed at 600 °C has a slightly higher energy band gap compared with sample heated at 400 °C. This might be attributed to differences in crystallite size, which is twice bigger for ceramic pigment obtained at 600 °C than for sample heat treated at 400 °C (Table 2).

Color changing is very intensive with heat treatment of $Ce_{0.9}Pr_{0.1}O_2$. It is obvious from the corresponding $L^*a^*b^*$ coordinates (Table 2).

The color change of $Ce_{0.9}Pr_{0.1}O_2$ due to heating can be expressed by L^*a^* diagram (Fig. 6) keeping in mind that the b^* coordinates vary in the narrow range ($33.5 < b^* < 35.5$). The increasing contribution of magenta is noticeable with lightness decreasing (L^*) in the same time. Therefore, the color shifted toward red hue (increasing a^*) becoming more saturated (decreasing L^*) with the raising temperature.

The red color of the Pr-doped ceria is assigned to a charge transfer from the ligand orbitals to the praseodymium cation [4]. The electronic spectra arise due to the electron transfer from the ligand orbitals to the localized $4f^1$ level of the Pr^{4+} cation [21]. The position of the absorption edge depends crucially on the praseodymium valent state and its concentration in ceria lattice. As-prepared sample and sample annealed at low temperature (200 °C) still contained

Table 2
Calculated band gap and color measurement for samples treated at different temperatures.

Temperature (°C)	Band gap	Color measurement		
	Eg (eV)	L^*	a^*	b^*
20	3.17	77.35	7.96	33.55
200	3.14	73.41	11.89	35.53
400	2.02	45.94	26.27	34.09
600	2.06	34.86	30.14	35.39

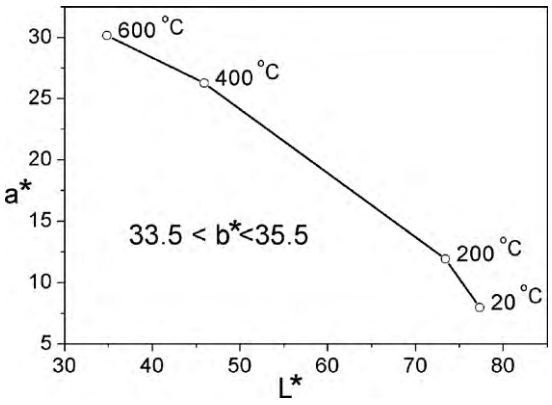

Fig. 6. Diagram of $Ce_{0.9}Pr_{0.1}O_2$ color change depending of temperature.

high amount of Ce^{3+} and Pr^{3+}, which increase the band gap, resulting in yellow-orange color.

4. Conclusion

In summary, $Ce_{1-x}Pr_xO_{2-\delta}$ solid solution ($x = 0.10$) was prepared by SPRT method that is easy to handle and low cost. It was found that the ceria powders with Pr dopant up to 10% are solid solution with fluorite structure. Particle size lies in the nanometric range. They exhibited larger lattice parameter than polycrystalline material due to presence of Ce^{3+}, Pr^{3+} ions and O^{2-} vacancies. However, increasing temperature results in crystal growth, which led to increasing absorption and shifting the absorption edge towards lower energy. As a consequence, dominant wavelength of the color is shifted towards red hue, becoming more saturated with temperature.

Acknowledgements

The authors are grateful to the Ministry of Science and Technological Development of Serbia, and A. von Humboldt Foundation, Germany, for the support.

References

[1] R.A. Eppler, in: L.L. Hench, D.B. Dove (Eds.), Physics of Electronic Materials, Part B, Marcel Dekker, New York, 1972, p. 1021.
[2] R. Olazcuaga, G. Le Polles, A. El Kira, G. Le Flem, P. Maestro, J. Solid State Chem. 71 (1987) 570.
[3] N. Maso, H. Beltran, R. Munoz, B. Julian, J.B. Carda, P. Escribano, E. Cordoncillo, J. Am. Ceram. Soc. 86 (2003) 426.
[4] S.T. Aruna, S. Ghosk, K.C. Patil, Int. J. Inorg. Mater. 3 (2001) 387.
[5] P. Sulcova, M. Trojan, Thermochim. Acta 395 (2002) 251.
[6] S.F. Santos, M.C. De Andrade, J.A. Sampaio, A.B. da Luz, T. Ogasawara, Dyes Pigments 75 (2007) 574.
[7] Y. Lunxiang, W. Yanqin, P. Guangsheng, K. Yuri, G. Aharon, J. Colloid Interface Sci. 246 (2002) 78.
[8] Y. Zhow, R.J. Philips, J.A. Switzer, J. Am. Ceram. Soc. 78 (1995) 981.
[9] P. Sulcova, Dyes Pigments 47 (2000) 285.
[10] P. Shuk, M. Greenblatt, Solid State Ionics 116 (1999) 217.
[11] F. Bondioli, A.M. Ferrari, L. Lusvarghi, T. Manfredini, S. Nannarone, L. Pasquali, G. Selvaggi, J. Mater. Chem. 15 (2005) 1061.
[12] S. Boskovic, D. Djurovic, Z. Dohcevic-Mitrovic, Z.V. Popovic, M. Zinkevich, F. Aldinger, J. Power Sources 145 (2005) 237.
[13] S. Boskovic, S. Zec, M. Ninic, J. Dukic, B. Matovic, D. Djurovic, F. Aldinger, J. Optoelectron. Adv. Mater. 10 (2008) 515.
[14] W. Hall, G.K. Williamson, Acta Metall. 1 (1953) 22.
[15] X.D. Liu, H.Y. Zhang, K. Lu, Z.Q. Hu, J. Phys. Condens. Matter 6 (1994) L947.
[16] Y.H. Zhao, K. Zhang, K. Lu, Phys. Rev. B 56 (1997) 14322.
[17] W. Qin, Z.H. Chen, P.Y. Huang, Y.H. Zhuang, J. Alloys Compd. 292 (1999) 230.
[18] A. Shannon, Acta Crystallogr. A32 (1976) 751.
[19] E. Spanier, R.D. Robinson, F. Zhang, S.W. Chan, I.P. Herman, Phys. Rev. B 64 (2001) 245407.
[20] D. Segal, K. Fujiwara, K. Machida, G. Adachi, T. Sakata, H. Mori, Chem. Mater. 9 (1997) 2197.
[21] H.E. Hoefdraad, J. Inorg. Nucl. Chem. 37 (1975) 1917.